IODP
INTERNATIONAL OCEAN
DISCOVERY PROGRAM

Check for updates

Contents

Data report: evaluation of shipboard magnetostratigraphy by alternating field demagnetization of discrete samples, Expedition 361, Site U1475[1]

J. Just[2] and the Expedition 361 Scientists[3]

Abstract

The paleomagnetic shipboard data of International Ocean Discovery Program Site U1475, with a record reaching back to approximately 7 Ma, allowed for the identification of major magnetic polarity chrons and subchrons back to ~3.5 Ma. However, the natural remanent magnetization (NRM) was very weak, and transitional intervals with unclear polarity were as thick as several meters. The midpoints of these transitional intervals were reported in the shipboard results without decimal places because of the poor data quality. To evaluate and possibly refine the shipboard magnetostratigraphy, subsampling was performed across the polarity transitions. Detailed alternating field (AF) demagnetization experiments were conducted on these discrete samples and were complemented by anhysteretic remanent magnetization acquisition measurements and subsequent demagnetization. AF demagnetization data of NRM were analyzed using anchored principal component analysis (PCA) to obtain the characteristic remanent magnetization. These PCA results generally confirm the smoothed signal across polarity transitions at Site U1475. However, the midpoint depths of the top of the Keana Subchron, the Gauss-Matuyama and Matuyama-Brunhes boundaries, and the base of the Olduvai Subchron were adjusted.

Introduction

Sediment cores from International Ocean Discovery Program (IODP) Expedition 361 Site U1475 (41°25.61′S, 25°15.64′E; 2669 m water depth) located at the Agulhas Plateau provide a continuous sedimentary record of the past approximately 7 My (see the **Site U1475** chapter [Hall et al., 2017]). These carbonate-rich sediments have a low concentration of magnetic minerals and therefore a weak paleomagnetic signal. Although we could identify major paleomagnetic chrons and subchrons, the precise position of their boundaries was difficult to determine because changes in inclinations were stretched over 1–2 m and sometimes up to 5 m (Figure **F1**). Such thick intervals and assumed sedimentation rates of ~3 cm/ky (see the **Site U1475** chapter [Hall et al., 2017]) would correspond to a duration of 30–60 ky, whereas observed reversal processes are generally much faster in other archives. In particular, for the Matuyama–Brunhes transition, durations between a few centuries (e.g., Just et al., 2019; Macrì et al., 2018; Sagnotti et al., 2016) and 5–10 ky (e.g., Channell, 2017; Valet and Fournier, 2016; Xuan et al., 2016) have been observed. The polarity transition at the base of Jaramillo Subchron was recently found to have occurred within less than 3 ky (Just et al., 2019).

Varying durations for the polarity transitions may result from regional expressions of nondipole components of the Earth's magnetic field (Leonhardt and Fabian, 2007); however, the apparently very long durations at Site U1475 likely result from depositional, compositional, or analytical effects. Virtually longer transitions could be related to the recording process in the sediment, for example, a low potential to record field changes when magnetic mineral concentrations are low or when the Earth magnetic field dipole component is weak (e.g., Valet and Fournier, 2016). Moreover, a deep lock-in zone (Shcherbakov and Shcherbakova, 1987) in combination with low sedimentation rates would result in an averaged recorded paleomagnetic signal within the sample volume (e.g., Roberts et al., 2013; Valet and Fournier, 2016). Smoothed transitions could also result from magnetic overprint imparted by the Earth's

Figure F1. Characteristic remanent magnetization (ChRM) inclinations of discrete samples across magnetic polarity zone boundaries compared with shipboard inclination data. Polarity is based on shipboard (left) and discrete sample (right) data. Black (white) stands for normal (reversed) polarity, and transitional phases are indicated by hatched pattern. Inner left column shows shipboard individual measurements (dots) with a 5-point running average (line). Inner right column shows discrete sample ChRM inclinations with maximum angular deviations (MADs) <15° in black, joined by a line. PCA inclinations with MADs >15° are shown as gray crosses. Arrows point toward the midpoint depths of the two data sets. CCSF = core composite depth below seafloor.
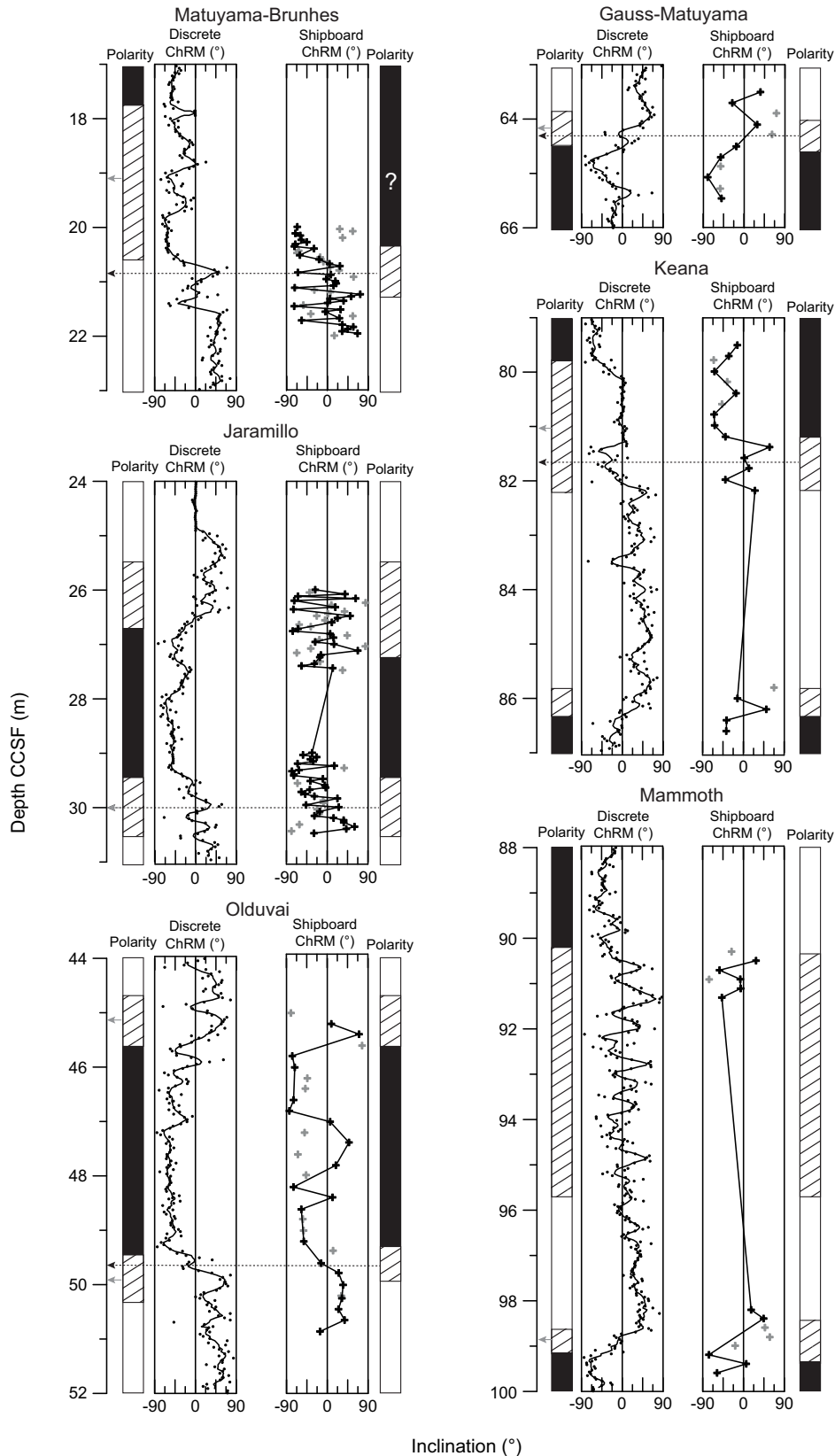
magnetic field or from the coring process (Richter et al., 2007). Core halves were subjected to a soft alternating field (AF) demagnetization treatment (25 mT) on board to minimize the latter overprinting effects. Smoothing could also be related to the response curve of the magnetometer, resulting in averaging of data across 20 cm of the sediment core (Richter et al., 2007), but this cannot account for the smearing of directions across meter scales.

To evaluate whether all viscous and coring overprints were removed by the shipboard AF treatment and to refine the shipboard magnetostratigraphy, discrete samples from the working halves were taken across polarity zone boundaries and subjected to detailed AF demagnetization experiments. These data were then analyzed by principal component analysis (PCA) (Kirschvink, 1980), and the characteristic remanent magnetization (ChRM) was calculated for each sample.

Materials and methods

In total, 269 discrete 8 cm^3 cube samples were collected from working halves of the spliced core composite. Sampling focused on the Gauss–Matuyama and Matuyama–Brunhes polarity transitions, as well as on the base and top of the Mammoth, Keana, Olduvai, and Jaramillo Subchrons, which were identified in the shipboard magnetic data (see the **Site U1475** chapter [Hall et al., 2017]). Cube samples were measured using a 2G cryogenic superconducting rock magnetometer at the University of Bremen (Germany). The natural remanent magnetization (NRM) was demagnetized using 12 AF steps between 5 and 100 mT peak fields. Afterward, an anhysteretic remanent magnetization (ARM) was imparted using a 100 mT AF and a 50 µT bias field, and the samples were subsequently demagnetized using the same 12 AF steps. PCA of NRM demagnetization data was performed using Puffinplot software (Lurcock and Wilson, 2012) to compute the ChRM. Because the demagnetization data of some samples cluster at stable components (cf. Figure **F2C**), performing PCA without using the origin as an anchoring point would result in random directions. We therefore chose the PCA anchored to the origin for the analyses. The number of steps included was adapted to data quality of individual samples and varies between four and six steps. The maximum angular deviation (MAD) of the PCA inclinations provides further quality control of the computed directional data. Because data were not corrected for core orientations, we present here only the inclination.

Results

Magnetic intensities of NRM (see U1457NRM.xlsx in **Supplementary material**) are on the order of 10^{-1} to 10^{-2} mA/m, which is only a factor of 10–100 higher than the sample handler magnetization. Consequently, demagnetization diagrams are of mixed quality and are noisy for low-intensity samples. Nevertheless, even some of the weak samples show clustering inclinations for successive demagnetization steps so that ChRM with acceptable MAD values <15° have been computed (Figure **F2**) using the anchored PCA approach. ARM varies between 1 and 10^{-1} mA/m (see

U1475ARM.xlsx and U1475ARMdemag.xlsx in **Supplementary material**).

Figure **F1** displays the shipboard split core inclination data next to the ChRM of discrete samples (see U1475ChRM.xlsx in **Supplementary material**) and the inferred polarity from both data sets. Shipboard and refined polarity boundary midpoints are presented in Table **T1**. It should be noted that because of the noisy character of the data, the shipboard midpoint depths (see the **Site U1475** chapter [Hall et al., 2017]) were reported in meters without decimal places.

Discrete samples with MAD values <15° are plotted in black and connected by a line, and samples with MAD values >15° (poor quality) are indicated in gray. At the base of the Mammoth Subchron, the polarity transition in the shipboard data is reproduced by the discrete samples (midpoint depth = ~99 m), whereas at its top, subsampling was not sufficient to capture the transition. In the shipboard data, the transition is stretched over some meters. Additionally, the base of the Keana Subchron was not captured in the discrete sample measurements. At the top of the Keana Subchron, the polarity switch from reversed to normal polarity appears sharper than in the split core data (82.2–81.2 m) with a midpoint depth of 81.7 m. At the top of the Gauss Chron, the midpoint of the polarity boundary at ~64 m from the shipboard data is corroborated. For both the base of the Olduvai (~50 m) and the Jaramillo (~30 m) Subchrons, the ChRM parallels the change in the shipboard inclination. For the Olduvai Subchron, the transition appears to be narrower in the discrete samples (49.8–49.2 m) with a derived midpoint depth of 49.5 m. The tops of Olduvai and Jaramillo Subchrons are inconclusive from the discrete samples. For the Matuyama–Brunhes boundary, a change in inclination corresponds to the shipboard data. The transitional interval was previously postulated between 20.8 and 17.8 m (see the **Site U1475** chapter [Hall et al., 2017]) (Figure **F1**). In light of the new discrete samples, it appears that the Matuyama–Brunhes transition only spans 21.2–20.5 m and has a corresponding midpoint depth of 20.8 m. However, the transitional interval visible in the shipboard split core data is not wholly covered by the subsamples, which leaves some uncertainty.

Concluding remark

The new discrete sample demagnetization data set largely parallels the shipboard data and supports the shipboard magnetostratigraphy. Some transitional zones appear thinner in the discrete sample data and lead to revised midpoint depths.

Acknowledgments

Figure F2. Results of alternating field (AF) demagnetization for selected samples with different demagnetization behaviors. For each sample, four panels are shown: (1) intensity after incremental AF demagnetization; (2) intensity, inclination, and declination for each field step, as well as the field steps used for PCA (stars); (3) equal area projections; and (4) Zijderfeld diagrams for demagnetization data. For the latter, blue lines indicate the fitted PCA inclination and declinations, which are also given in an inset together with the maximum angular deviation (MAD). A. Sample 361-U1475E-3H-3W, 142–144 cm, shows a clear demagnetization path. B. Although data are noisy, characteristic directions with a MAD of 7° were obtained for Sample 361-U1475-2H-2W, 54–56 cm. C. For Sample 361-U1475E-4H-2W, 46–48 cm, data of individual field steps cluster and a ChRM direction with MAD <10° was computed. D. Sample 361-U1475B-10H-3W,108–110 cm, shows consistent but changing directions upon demagnetization, indicating the stepwise removal of various overprints. Analyses and graphics were produced using Puffinplot (Lurcock and Wilson, 2012).
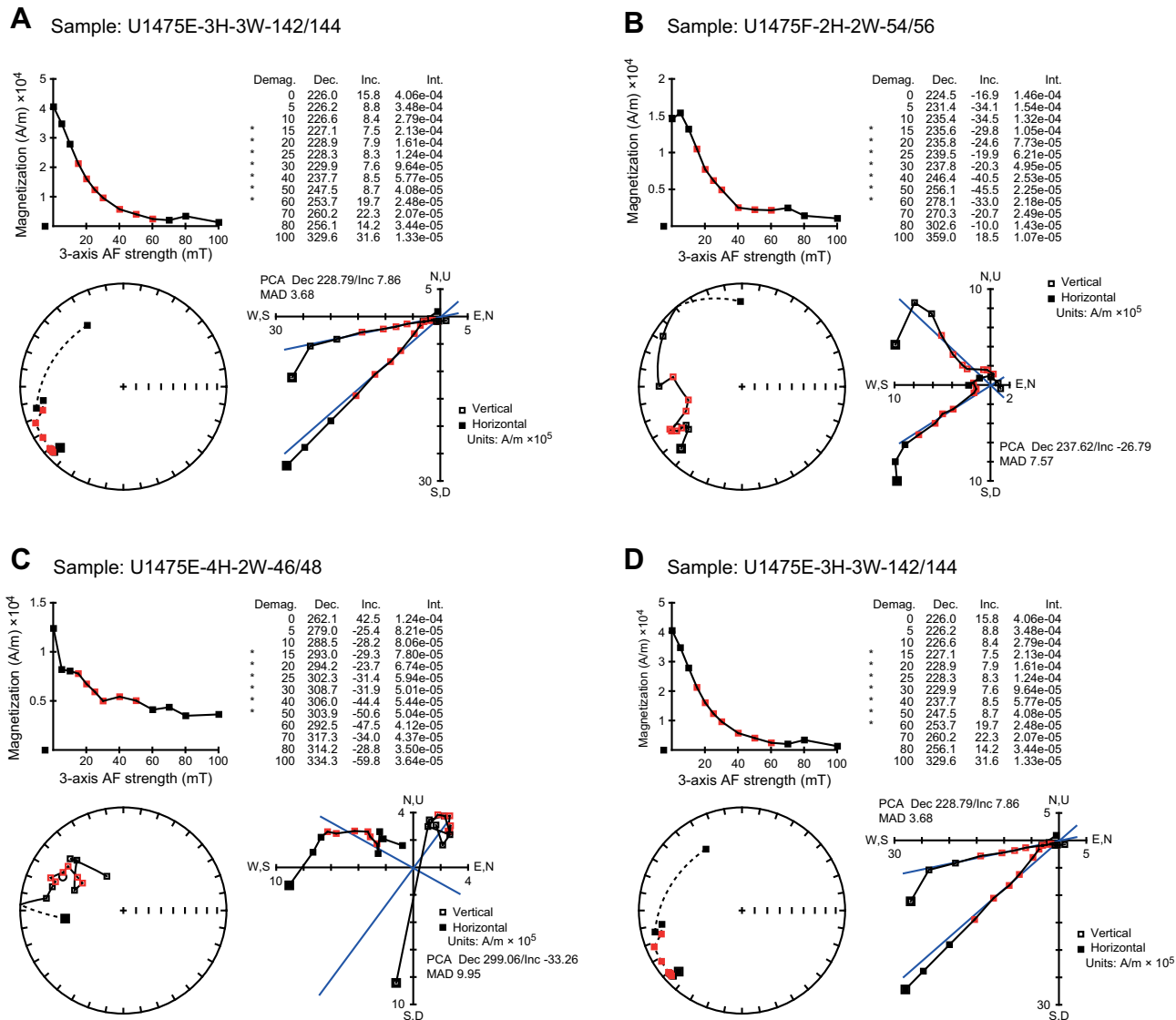
A   Sample: U1475E-3H-3W-142/144

B   Sample: U1475F-2H-2W-54/56

C   Sample: U1475E-4H-2W-46/48

D   Sample: U1475E-3H-3W-142/144

Table T1. Revised polarity reversal midpoint depths. **Download table in CSV format.**

References

Channell, J.E.T., 2017. Complexity in Matuyama-Brunhes polarity transitions from North Atlantic IODP/ODP deep-sea sites. *Earth and Planetary Science Letters*, 467:43–56. **https://doi.org/10.1016/j.epsl.2017.03.019**

Hall, I.R., Hemming, S.R., LeVay, L.J., Barker, S., Berke, M.A., Brentegani, L., Caley, T., Cartagena-Sierra, A., Charles, C.D., Coenen, J.J., Crespin, J.G., Franzese, A.M., Gruetzner, J., Han, X., Hines, S.K.V., Jimenez Espejo, F.J., Just, J., Koutsodendris, A., Kubota, K., Lathika, N., Norris, R.D., Periera dos Santos, T., Robinson, R., Rolinson, J.M., Simon, M.H., Tangunan, D., van der Lubbe, J.J.L., Yamane, M., and Zhang, H., 2017. Site U1475. *In*

Hall, I.R., Hemming, S.R., LeVay, L.J., and the Expedition 361 Scientists, *South African Climates (Agulhas LGM Density Profile).* Proceedings of the International Ocean Discovery Program, 361: College Station, TX (International Ocean Discovery Program). **https://doi.org/10.14379/iodp.proc.361.104.2017**

Just, J., and the Expedition 361 Scientists, 2020. Supplementary material, **https://doi.org/10.14379/iodp.proc.361.202Supp.2020**. *Supplement to* Just, J., and the Expedition 361 Scientists, 2020.Data report: evaluation of the shipboard magnetostratigraphy by alternating field demagnetization of discrete samples, Expedition 361, Site U1475. *In* Hall, I.R., Hemming, S.R., LeVay, L.J., and the Expedition 361 Scientists, *South African Climates (Agulhas LGM Density Profile).* Proceedings of the International Ocean Discovery Program, 361: College Station, TX (International Ocean Discovery Program). https://doi.org/10.14379/iodp.proc.361.202.2020

Just, J., Sagnotti, L., Nowaczyk, N.R., Francke, A., and Wagner, B., 2019. Recordings of fast paleomagnetic reversals in a 1.2 Ma greigite-rich sediment archive from Lake Ohrid, Balkans. *Journal of Geophysical Research: Solid Earth*, 124(12):12445–12464. **https://doi.org/10.1029/2019JB018297**

Kirschvink, J.L., 1980. The least-squares line and plane and the analysis of palaeomagnetic data. *Geophysical Journal of the Royal Astronomical Society,* 62(3):699–718. **https://doi.org/10.1111/j.1365-246X.1980.tb02601.x**

Leonhardt, R., and Fabian, K., 2007. Paleomagnetic reconstruction of the global geomagnetic field evolution during the Matuyama/Brunhes transition: iterative Bayesian inversion and independent verification. *Earth and Planetary Science Letters*, 253(1–2):172–195. **https://doi.org/10.1016/j.epsl.2006.10.025**

Lurcock, P.C., and Wilson, G.S., 2012. PuffinPlot: a versatile, user-friendly program for paleomagnetic analysis. *Geochemistry, Geophysics, Geosystems,* 13(6):Q06Z45. **https://doi.org/10.1029/2012GC004098**

Macrì, P., Capraro, L., Ferretti, P., and Scarponi, D., 2018. A high-resolution record of the Matuyama-Brunhes transition from the Mediterranean region: the Valle di Manche section (Calabria, Southern Italy). *Physics of the Earth and Planetary Interiors*, 278:1–15. **https://doi.org/10.1016/j.pepi.2018.02.005**

Richter, C., Acton, G., Endris, C., and Radsted, M., 2007. *Technical Note 34: Handbook for Shipboard Paleomagnetists.* Ocean Drilling Program. **https://doi.org/10.2973/odp.tn.34.2007**

Roberts, A.P., Tauxe, L., and Heslop, D., 2013. Magnetic paleointensity stratigraphy and high-resolution Quaternary geochronology: successes and future challenges. *Quaternary Science Reviews*, 61:1–16. **https://doi.org/10.1016/j.quascirev.2012.10.036**

Sagnotti, L., Giaccio, B., Liddicoat, J.C., Nomade, S., Renne, P.R., Scardia, G., and Sprain, C.J., 2016. How fast was the Matuyama-Brunhes geomagnetic reversal? A new subcentennial record from the Sulmona Basin, central Italy. *Geophysical Journal International*, 204(2):798–812. **https://doi.org/10.1093/gji/ggv486**

Shcherbakov, V.P., and Shcherbakova, V.V., 1987. On the physics of acquisition of postdepositional remanent magnetization. *Physics of the Earth and Planetary Interiors*, 46(1–3):64–70. **https://doi.org/10.1016/0031-9201(87)90171-3**

Valet, J.-P., and Fournier, A., 2016. Deciphering records of geomagnetic reversals. *Reviews of Geophysics*, 54(2):410–446. **https://doi.org/10.1002/2015RG000506**

Xuan, C., Channell, J.E.T., and Hodell, D.A., 2016. Quaternary magnetic and oxygen isotope stratigraphy in diatom-rich sediments of the southern Gardar Drift (IODP Site U1304, North Atlantic). *Quaternary Science Reviews*, 142:74–89. **https://doi.org/10.1016/j.quascirev.2016.04.010**